Optimal design of a pot core rotating transformer

Optimal Design of a Pot Core Rotating Transformer

J.P.C. Smeets, D.C.J. Krop, J.W. Jansen, M.A.M. Hendrix, E.A. Lomonova
Department of Electrical Engineering, Electromechanics and Power Electronics
Eindhoven University of Technology, Eindhoven, The Netherlands
Email: j.p.c.smeets@tue.nl

***Abstract*—This paper discusses the optimal design of a pot core rotating transformer to replace wires and slip rings in mechatronic systems by means of contactless energy transfer. Analytic models of the transformer are derived in the electromagnetic and thermal discipline. The models are compared with both 2D/3D FEM simulations and measurements. The analytical models are combined and used in a multi-objective sequential quadratic programming algorithm to find the minimal Pareto front in terms of volume and power loss for comparison of the adjacent and coaxial winding topologies. Finally, the optimization algorithm is used for the design of two prototype rotating transformers for a power transfer of 1kW peak, rotating at 4000 rpm. The prototypes are manufactured and tested in an experimental setup.**

I. Introduction

Contactless energy transfer (CET) plays an important role in modern advanced mechatronic systems as a solution for cable slabs and slip rings. This paper focuses on a CET solution for the transfer of power to a rotating part of a device. Examples can be found in robotic [1] and aerospace applications [2]. Usually, wires and slip rings are used to transfer power to the rotating part. Wires have the disadvantages that they suffer from wear, increase stiffness and limit 360 free rotation. Slip rings have a limited lifetime and create dust particles due to contact wear and frequent maintenance is required [3].

A solution to overcome the disadvantage of wires and slip rings is a CET system by means of a rotating transformer. The contactless solutions overcomes contact wear, and thereby, frequent maintenance is avoided. Ferrite core are implemented in the system to improve the power transfer capability over a small airgap.

The axial rotating and pot core transformer geometry can be used for a rotating transformer. Both are investigated in [4], concluding that the pot core rotating transformer, Fig.1, gives better performance indices in terms of flux density, magnetic coupling and minimal core and winding losses. Therefore, this geometry is investigated in this paper.

The paper presents a fast design optimization tool for a rotating pot core transformer. It is achieved by deriving an electromagnetical and thermal model of the rotating transformer, and combing the models in an optimization procedure. A multi-objective optimization is conducted to define the optimal winding topology [5], and to design a rotating transformer for the transfer of 1 kW with an output voltage of 50 Vdc, rotating at 4000 rpm. Finally, prototypes are manufactured using a commercially available pot core. The prototypes are used to verify the derived transformer models.

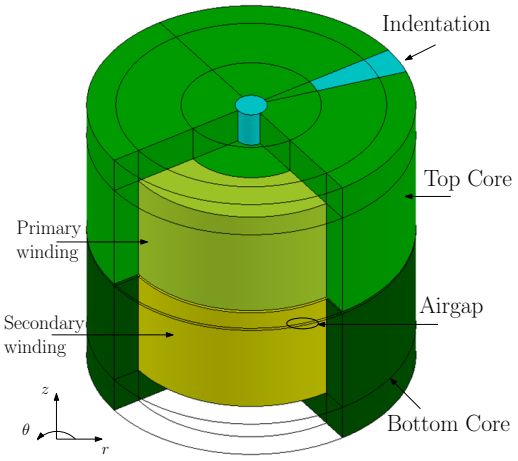

Fig. 1. Pot core rotating transformer.

II. Rotating Pot Core Transformer

A. Transformer Geometry

The initial size of a pot core rotating transformer can be determined by Faraday's law of induction and Ampere's circuital law. Combining those laws gives a design expression for the power transfer

$$P = \pi J S k_f f B_{peak} A_e, \tag{1}$$

based on the current density, J, the frequency of the applied voltage, f, the peak flux density, B_{peak}, the filling factor of the winding, k_f, and the geometric parameters S and A_e, representing the winding area and the cross section of the inner core, respectively. An illustration of the geometric parameters is shown in Fig. 2 and listed in Table I.

In each core an indentation can be found, to guide the wires of the winding out the core, which creates an incomplete axissymmetric layout. The effect of the indentation on the power transfer during rotation is investigated by a 3D FEM model [6]. Figure 3a-d shows the response of the secondary voltage for a changing load resistance for different relative positions of the indentations in the core halves. In each figure, an extra curve is inserted and identical responses for the different angular positions have been found. Concluding that an axissymmetric geometry can be assumed for further analysis.

978-1-4244-5287-3/10/$26.00 ©2010 IEEE

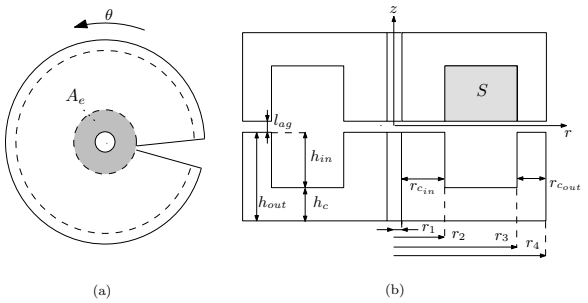

Fig. 2. Geometry of the pot core rotating transformer, (a) top view and (b) cross section.

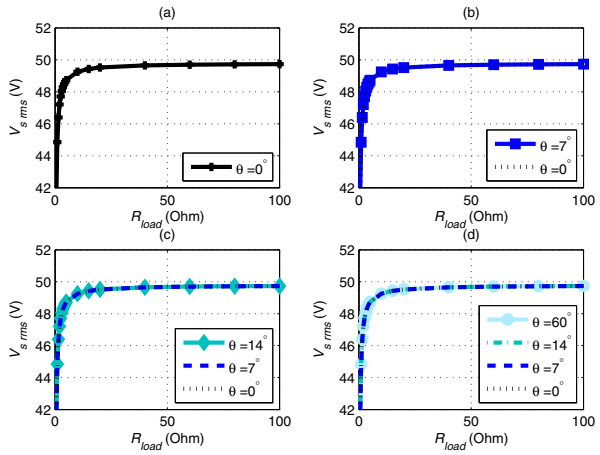

Fig. 3. Secondary voltage characteristics for different relative angular positions of the indentations in the core.

B. Winding Topologies

The pot core transformer can be established with two winding topologies [2]. The first winding topology to be considered is the adjacent winding topology, which is shown in Fig. 4a. In this topology, each winding is placed in an own core half. From a geometric point of view, it is less complex to rotate and another physical medium can be placed between both core halves.

The second topology to be investigated is the coaxial winding topology, which is shown in Fig. 4b. The windings are placed around each other is this case, and therefore, the alignment of the transformer becomes more demanding, since small axial vibration can damage the windings.

III. Multi-physical Model

An analytical model for the pot core rotating transformer is derived in the electromagnetic and thermal disciplines. In this section, the models are explained per discipline in more detail for the rotating transformer with the adjacent winding topology. The models for the coaxial winding topology are derived in a similar way.

TABLE I
Geometrical parameters of Fig. 2 and Fig. 4

Parameter	Description
r_1, r_2, r_3, r_4	Radius of the different core parts
$r_{c_{in}}$	Length of the inner core part
$r_{c_{out}}$	Length of the outer core part
h_{out}	Outer height of a core half
h_{in}	Height of the winding area S
h_c	Thickness of the horizontal core part
l_{ag}	Length of the airgap
A_e	Effective core area
S	Winding surface
N_p	Number of turns on primary side
N_s	Number of turns on secondary side

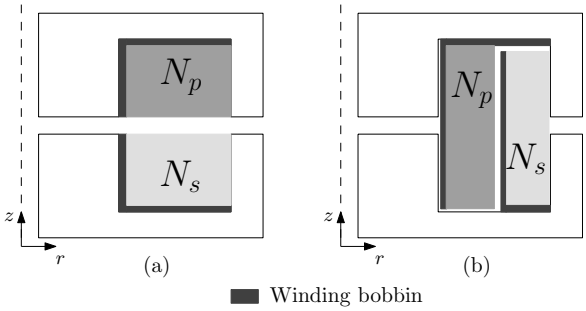

Fig. 4. Winding topologies for the pot core rotating transformer, (a) adjacent and (b) coaxial.

A. Magnetic model

A magnetic model is derived to calculate the inductances of the transformer. The magnetizing inductance, L_m, is calculated using a reluctance model. The model is shown in Fig. 5, where $\mathcal{R}$ presents the reluctance of the magnetic path and the subscripts c, ag and lk indicate the flux path in the core, airgap and leakage, respectively. The magnetizing inductance is calculated by

$$L_m = \frac{N_p^2}{2(\mathcal{R}_{c_a} + \mathcal{R}_{c_b} + \mathcal{R}_{c_c}) + \mathcal{R}_{ag_a} + \mathcal{R}_{ag_b}}. \tag{2}$$

The leakage flux lines in the rotating transformer do not have an a priori known path, therefore, it is inaccurate to model them with a reluctance network as well. The leakage inductance, L_{lk}, is calculated by the energy of the magnetic field in the winding volume

$$\frac{1}{2} L_{lk} I^2 = \frac{1}{2} \int_v \mathbf{B} \cdot \mathbf{H} dv, \tag{3}$$

which is equal to the magnetic energy of the leakage inductance [7]. An expression for the magnetic field strength is found by the magnetic circuit law. In the case of the adjacent winding topology, the magnetic field strength is expressed for the primary winding as function of the axial length

$$H(z) = \frac{N_p i_p}{(r_3 - r_2)} \frac{z}{h_{wp}}, \tag{4}$$

where h_{wp} is the height of the primary winding. A similar expression can be derived along the secondary winding. In

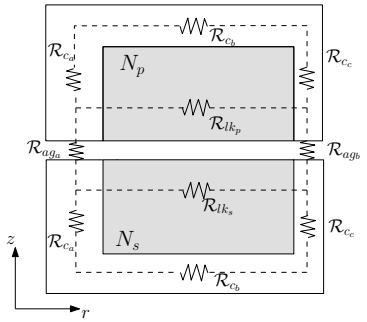

Fig. 5. Reluctance model of the rotating transformer with adjacent winding topology.

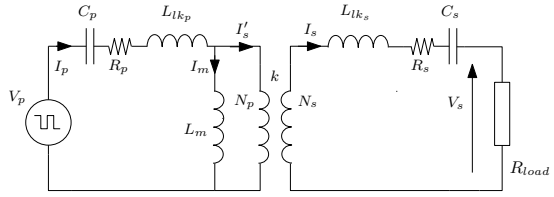

Fig. 6. Electric equivalent circuit of the rotating transformer.

the airgap a uniform mmf is assumed, defining the magnetic field strength by

$$H = \frac{N_p i_p}{l_{ag}}. \tag{5}$$

Combining (3)-(5), results in an expression for the total leakage inductance of the transformer seen from the primary side

$$L_{lk} = \mu_0 N_p^2 \frac{2\pi}{ln(r_3/r_2)} \left(\frac{h_{w_p} + h_{w_s}}{3} + l_{ag} \right). \tag{6}$$

B. Electric model

An electric equivalent circuit of the rotating transformer is derived to calculate the power losses in the transformer. The model is shown in Fig. 6. In the circuit, the rotating transformer is represented by the magnetizing and leakage inductances and a lossless transformer with winding ratio $a = N_p/N_s$ and coupling factor, k. Furthermore, winding resistance and resonance capacitances are inserted. The circuit is connected to a square wave input voltage source and an equivalent load resistance.

The winding resistance, R_p, R_s, consists of a dc and ac-resistance. An expression for the winding resistance in case of non-sinusoidal waveforms is derived in [8], based on Dowell's formula for ac-resistances.

To improve the power transfer of the transformer, resonant techniques are used [9]. A resonant capacitor is placed in series on both sides of the transformer:

- On the primary side, to create a zero crossing resonance voltage and thereby allowing the use of a half bridge inverter.

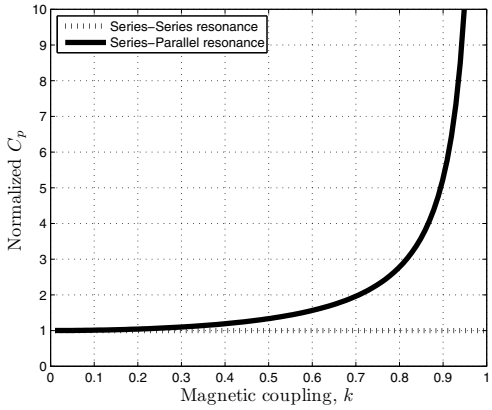

Fig. 7. Influence of the magnetic coupling on the primary resonance capacitance.

- On the secondary, to overcome the voltage drop across the leakage inductance and thereby improving the power transfer.

Furthermore, by a applying series resonance on the secondary side, the primary side is made unsensitive for coupling changes, for example caused by vibration during rotation. This can be illustrated by calculating the value of the primary resonance capacitance for a series and parallel resonance on the secondary side as shown in Fig. 7 for an increasing magnetic coupling [10]. A constant primary resonance capacitance can be obtained by applying series resonance on the secondary side,

The resonance technique creates a band pass filter around the resonance frequency to filter-out unwanted harmonics and thereby decreasing the ac-losses in the windings. The quality of this filter depends on the resonance frequency, leakage inductance and load resistance of the transformer and is defined by

$$Q = \frac{2\pi f_{res} L_{lk}}{R_{load}}. \tag{7}$$

The conduction and core losses are the main power losses in the rotating transformer. The conduction losses, P_{cond}, are calculated by

$$P_{cond} = I_{p_{rms}}^2 R_p + I_{s_{rms}}^2 R_s, \tag{8}$$

where $I_{p_{rms}}$ is the primary rms-current, which consists of the magnetizing current and the reflected load current. The core losses, P_{core}, are calculated by the Steinmetz equation

$$P_{core} = C_m C(T) f_{res}^x B^y V_{core}, \tag{9}$$

where C_m, x and y are material specified constants (for example C_m=7, x=1.4 and y=2.5 for the 3C81 core material). $C(T)$ is a temperature depending constant and is equal to 1 if the core temperature is $\pm 20^\circ$ around the ideal working temperature, which is $60^\circ C$ for the 3C81 core material. For a constant power transfer, the flux density can be calculated

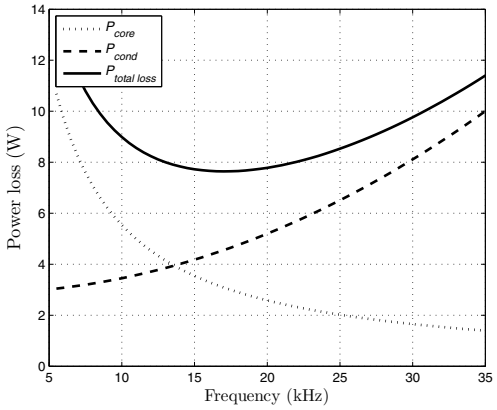

Fig. 8. Power losses as a function of the frequency for the P66/56 pot core.

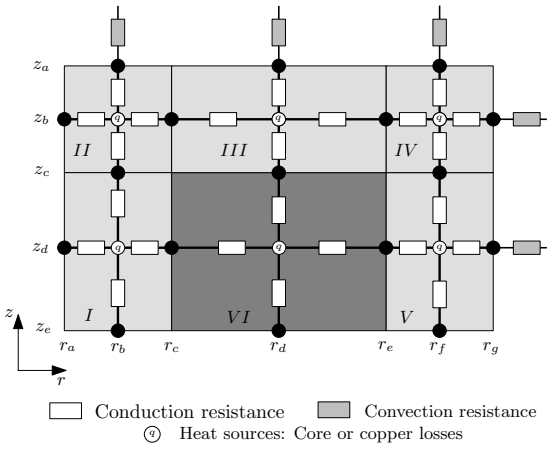

Fig. 9. Thermal equivalent circuit of the transformer.

as a function of frequency as indicated in (1). By varying the frequency an optimal working point with minimal losses can be found for a given geometry, as shown in Fig. 8 for the P66/56 pot core [11].

C. Thermal model

It is important to estimate the core temperature since the core and conduction losses cause a temperature rise in the core material, which has an optimal working temperature with minimal power losses. A thermal equivalent circuit of the core, shown in Fig. 9, is made using a finite-difference modeling technique, where the thermal resistance concept is used for deriving the heat transfer between the nodes [12].

The thermal model is derived by dividing the upper half of the geometry into six regions, where regions I till V represent the core and region VI represents the transformer winding. Five nodes are defined for each region and the heat transfer between the nodes is modeled by a thermal resistance. Conduction resistances are used to model heat transfer inside the regions and convection resistances are used to model the heat transfer between the border of the regions and the air. The conductive thermal resistance in z- and r- direction are calculated by

$$R_{th_z} = \frac{\triangle z}{\pi(r_o^2 - r_i^2)k}, \quad (10)$$

$$R_{th_r} = \frac{ln(r_o/r_i)}{2\pi k \triangle z}, \quad (11)$$

where k is the thermal conductivity, equal to 4.25 and 394 $\mathrm{Wm^{-1}K^{-1}}$ for the ferrite core and copper , respectively. The convective thermal heat resistance is calculated by

$$R_h = \frac{1}{hA}, \quad (12)$$

where h is the heat transfer coefficient obtained from the Nusselt-number, which is equal to 12.7 and 8.5 $\mathrm{Wm^{-2}K^{-1}}$ for the axial and radial boundaries of the pot core [12].

No heat transfer is assumed at left and lower boundary of the model, assuming a worst-case thermal situation, since the convection thermal resistances are the predominantly resistances in the model. The power losses in each region are presented by a heat source and inserted in the middle node of region. By calculating the heat transfer between each node, the temperature in the middle of each region is obtained. An ambient temperature of $20°C$ is assumed.

The multi-physical model is adapted for each winding topology and the two models are used to optimize the transformer design.

IV. Optimization algorithm

The analytical models are implemented in MATLAB and used in an optimization procedure to find the optimal transformer design in terms of both minimal volume and power losses for a constant power transfer of 1 kW and a secondary voltage of 50 V. A sequential quadratic programming algorithm is used to find the minimal Pareto front of the two objective functions [13]. Therefore, the weighted sum method for multi-objective problems is used

$$\begin{cases} min \quad F(x) = \sum_{m=1}^{N_{obj}} w_m f_m(x) & m = 1, ..., N_{obj} \\ \qquad\quad g_j(x) \leq 0 & j = 1, ..., J_{neq} \\ \qquad\quad h_k(x) = 0 & k = 1, ..., K_{eq} \\ \qquad\quad x_i^{lo} \leq x_i \leq x_i^{up} & i = 1, ..., N_{var} \end{cases} \quad (13)$$

The weights $w_m \in [0, ..., 1]$ are selected such that the sum of the weighting coefficients is always $\sum_{m=1}^{N_{obj}} w_m = 1$. This function finds the minimum of the objective functions subjected to the unequality, g_j, and equality constraints, h_k, within the lower and upper boundaries of the variables x_i. In the next sections the variables, constraints and objective functions are explained in more detail.

A. Variables

As shown in (1), the core dimensions, length of the airgap, number of turns and frequency are parameters which have influence on the design of the rotating transformer. The lower

TABLE II
LIMITS OF THE OPTIMIZATION VARIABLES.

min		var.		max
r_1	$<$	r_2	$\leqq$	r_{max}
r_2	$<$	r_3	$\leqq$	r_{max}
0	$<$	h_{in}	$\leqq$	h_{max}
0.5 mm	$\leqq$	l_{ag}	$\leqq$	2.0 mm
1	$\leqq$	N_p	$\leqq$	N_{max}
1	$\leqq$	N_s	$\leqq$	N_{max}
1 kHz	$\leqq$	f_{res}	$\leqq$	200 kHz

TABLE III
CONSTRAINTS

B_{core}	$\leqq$	B_{sat}
k	$\geqq$	0.6
V_p	$\leqq$	$V_{dc_{max}}$
J_n	$\leqq$	$J_{n_{max}}$
Q	$\geqq$	1
T_{core}	$\leqq$	$100°C$

and upper value of those variables is specified in Table II. Where N_{max} is the maximum number of turns, defined by

$$N_{max} = \frac{Sk_f}{A_{wire}}. \tag{14}$$

Parameters r_{max} and h_{max} limit the maximum core dimensions and, thereby, reduce the calculation time. Furthermore, the ratio between the inner and outer radial length and the thickness of the horizontal core part are fixed, based on existing pot cores dimensions [11]

$$r_{c_{out}} = 0.55 r_{c_{in}}, \tag{15}$$
$$h_c = 0.65 r_{c_{in}}, \tag{16}$$
$$r_1 = 2.7 \text{ mm}. \tag{17}$$

With constraint (17) the inner radius of the core is set to obtain a minimal hole in the middle of the transformer to mount the core. Other geometric parameters such as core material specifications and wire parameters are given as input parameters for the optimization function.

B. Constraints

For the electromagnetic and thermal properties of the rotating transformer, a number of constraints is introduced and listed in Table III.

C. Objective functions

The design optimization is conducted in terms of minimal volume and power losses, using the following objective functions

$$f_1(x) = \pi r_4^2 \cdot 2h_{out}, \tag{18}$$
$$f_2(x) = P_{cond} + P_{core}. \tag{19}$$

Both objectives are normalized by defining the two limits of the Pareto front, resulting in parameter sets x^{1*} and x^{2*} for the individual minimization of $f_1(x)$ and $f_2(x)$, respectively [14] (see Fig. 10). The normalized objective functions are

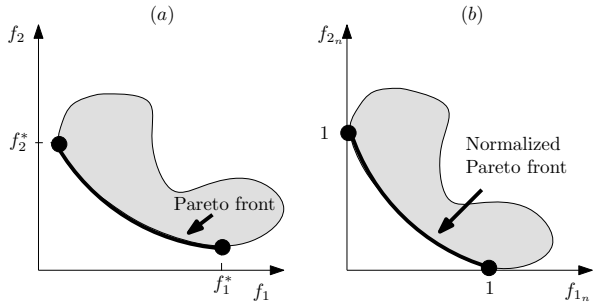

Fig. 10. Pareto front before (a) and after (b) normalization.

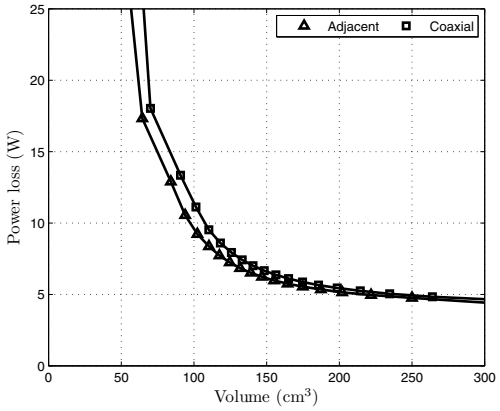

Fig. 11. Pareto front for optimal design in terms of volume and power losses.

$$f_{1_n}(x) = \frac{f_1(x) - f_1(x^{1*})}{f_1(x^{2*}) - f_1(x^{1*})}, \tag{20}$$
$$f_{2_n}(x) = \frac{f_2(x) - f_2(x^{2*})}{f_2(x^{1*}) - f_2(x^{2*})}. \tag{21}$$

The normalization allows an equal comparison of both winding topologies.

V. DISCUSSION OF THE OPTIMIZATION RESULT

By applying different combinations of weighing factors, a minimal Pareto front is found for both topologies, shown in Fig. 11. The Pareto front shows that the adjacent winding topology obtains lower power losses for the same core volume compared the coaxial winding topology. In the Pareto front two asymptotes can be obtained. A vertical asymptote for the minimal required core volume, limited by the maximal allowable core temperature, since the losses are increasing dramatically for a small core with a high frequency and high magnetic flux density. And a horizontal asymptote for the minimal power losses, which is based on an optimum in magnetic flux density, frequency and volume, comparable as shown in Fig. 8.

Detailed transformer parameters are given for two realistic extreme optimization cases for the coaxial and adjacent winding topology in Table IV. The objective functions

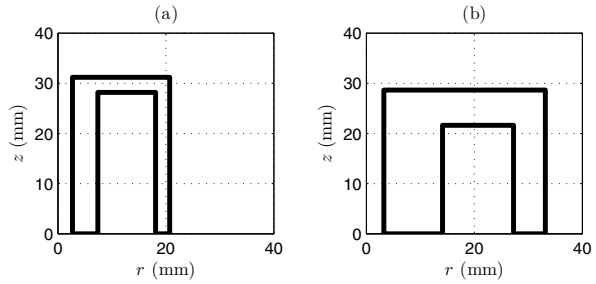

Fig. 12. Optimized core dimensions for the coaxial winding topology, (a) minimal volume and (b) minimal losses.

TABLE IV
TRANSFORMER PARAMETERS FOR TWO CASES WITH COAXIAL WINDING TOPOLOGY.

Parameter	Winding topology				Unit
	Coaxial		Adjacent		
	case 1	case 2	case 1	case 2	
$r_{c_{in}}$	5.6	16.2	4.7	16.1	mm
$r_{c_{out}}$	3.1	10.5	2.6	8.9	mm
r_4	23.9	42.6	20.7	37.6	mm
h_{out}	28.6	31.0	31.2	31.0	mm
l_{ag}	0.5	0.5	0.5	0.5	mm
S	311	195	302	203	mm^2
A_e	194	1456	149	1087	mm^2
V	102	354	84	274	cm^3
N_p	96	62	99	70	turns
N_s	10	6	10	7	turns
B_{core}	294	116	317	131	mT
f_{res}	20.4	10.7	24	11.2	kHz
L_{m_p}	3.38	8.63	2.70	8.35	mH
L_{Lk_p}	0.05	0.05	0.83	0.65	mH
L_{lk_s}	0.55	0.48	8.45	6.55	μH
k	0.98	0.99	0.76	0.93	-
P_{loss}	10.7	4.1	12.9	4.2	W
T_{core}	48.6	30.7	52.8	32.5	°C

are defined as $90\%f_{1_n}(x) + 10\%f_{2_n}(x)$ for case 1 and $10\%f_{1_n}(x) + 90\%f_{2_n}(x)$ for case 2. In other words, the volume is minimized in case 1 and the power losses are minimized in case 2. The upper half of the cross section of two coaxial cases is shown in Fig. 12. The core dimensions of the adjacent winding topology are almost identical to the coaxial winding topology and therefore not shown.

Comparing the optimization results the following observations are made:

- The winding area remains approximately the same during the optimization to be able to contain the optimal amount of windings. Because the adjacent winding topology uses the winding area more efficient, the total transformer volume of this topology is slightly lower compared to the coaxial winding topology.
- The magnetizing inductances of both winding topologies are comparable for the different cases.
- The leakage inductance of the coaxial winding topology is approximately 15 times lower compared to the adjacent winding topology. This is because both windings of the coaxial winding topology share an identical magnetic flux path, which is not the case in the adjacent winding topology. Resulting in a higher magnetic coupling for the coaxial winding topology.
- The winding ratio is the same in the four cases, because of the fixed secondary voltage and the maximized primary voltage. The optimization algorithm maximizes the primary voltage, to reduce the primary current and thereby the losses.
- In adjacent winding topology, a lower frequency and magnetic flux density is obtained compared to the adjacent winding topology, corresponding to the relation between the geometry, frequency and flux density as given in (1).
- The ratio between power losses and transformer volume is lower for the adjacent winding topology compared to the coaxial winding topology.
- The temperature is depending on the power losses and core volume and is thus higher in the adjacent winding topology compared to the coaxial winding topology.

Overall, minimal losses can be obtained in a relative larger core. The adjacent winding topology is favorable because it uses the winding area more efficient, resulting in a lower magnetizing current and thereby, lower losses, as shown in the Pareto front.

TABLE V
P66/55 POT CORE DIMENSIONS.

Parameter	Dimension	Unit
$r_{c_{in}}$	10.8	mm
$r_{c_{out}}$	5.9	mm
r_4	33.2	mm
h_{out}	28.7	mm
l_{ag}	0.5	mm
S	286	mm^2
A_e	583	mm^2
V	199	cm^3

VI. EXPERIMENTAL VERIFICATION

To verify the optimization algorithm and design models, a rotating transformer is manufactured for each winding topology. The transformer designs are retrieved from the optimization algorithm in which the core and conduction losses are minimized for a peak power transfer of 1 kW. In this particular case, a Ferroxcube P66/56 core is used and, therefore, the core dimensions are fixed, specified in Table V. The pot core consist of the material 3C81 [11], a special developed MnZn ferrite for high power applications below a frequency of 200 kHz, with minimal power losses around 60°C. The material has a low saturation level, hence in this paper a saturation level of 350 mT is assumed. A picture of the manufactured transformers is shown in Fig. 13.

The transformer parameters are shown in Table VI and VII for the adjacent and coaxial winding topology, respectively. The parameters are compared with FEM simulations [6] and the inductances are measured with the HP 4194A impedance analyzer. Those inductances measurements, in combination with the analytical and numerical calculated inductances are

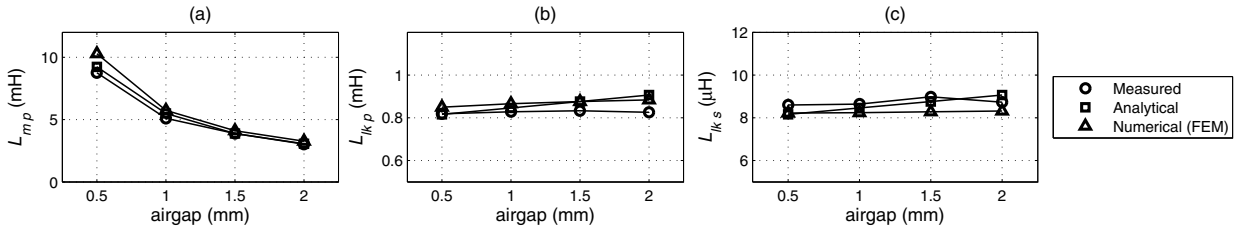

Fig. 14. The (a) primary magnetizing inductance, (b) primary leakage inductance and (c) secondary leakage inductance of the adjacent winding rotating transformer.

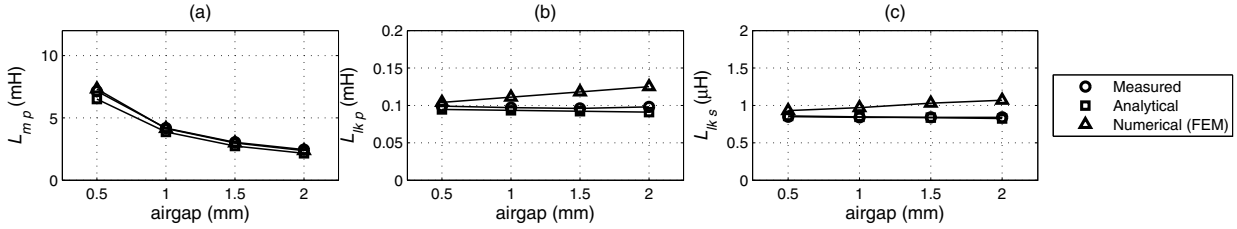

Fig. 15. The (a) primary magnetizing inductance, (b) primary leakage inductance and (c) secondary leakage inductance of the coaxial winding rotating transformer.

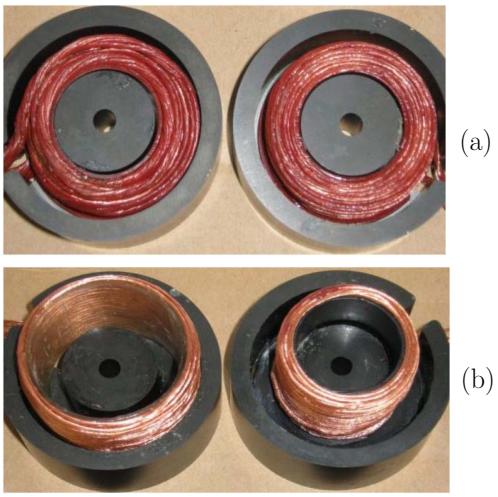

Fig. 13. Manufactured transformers (a) adjacent winding topology and (b) coaxial winding topology.

TABLE VI
OPTIMIZED TRANSFORMER PARAMETERS FOR THE ADJACENT WINDING TOPOLOGY.

Parameter	Optimization	FEM	Measurement	Unit
N_p	100	-	-	turns
N_s	10	-	-	turns
l_{ag}	0.5	-	-	mm
f_{res}	18.6	-	-	kHz
B_{core}	104	106	-	mT
L_{m_p}	9.2	10.5	8.8	mH
L_{Lk_p}	0.82	0.89	0.82	mH
L_{lk_s}	8.2	8.9	8.6	μH
k	0.92	0.92	0.91	-
P_{loss}	9.4	10	-	W
T_{core}	59	56	-	°C

TABLE VII
OPTIMIZED TRANSFORMER PARAMETERS FOR THE COAXIAL WINDING TOPOLOGY.

Parameter	Optimization	FEM	Measurement	Unit
N_p	83	-	-	turns
N_s	8	-	-	turns
l_{ag}	0.5	-	-	mm
f_{res}	30.8	-	-	kHz
B_{core}	75	74	-	mT
L_{m_p}	6.8	7.3	7.1	mH
L_{Lk_p}	0.09	1.0	1.0	mH
L_{lk_s}	0.9	0.9	0.8	μH
k	0.99	0.99	0.99	-
P_{loss}	14.5	12	-	W
T_{core}	89	85	-	°C

shown in Fig. 14 and 15 over an increasing airgap for the adjacent and coaxial winding topology, respectively. The figures show that the leakage inductance of the coaxial winding topology is significantly lower compared to the adjacent winding topology. The difference in magnetizing inductance is caused by the different number of turns used in both manufactured transformers. Overall, a maximum error of 8% is obtained between the calculated parameters and numerical, respectively measured, parameters.

Comparison of the parameters of the prototype transformers, shows that minimal losses are obtained in the adjacent winding topology. This can be explained by the different number of turns which fit in the winding area of both topologies. Since the adjacent winding topology uses the winding area more efficiently, a higher number of turns is obtained which increases the magnetizing inductance and simultaneously decreases the magnetizing current and the resonance frequency. This results in lower core and conduction losses compared to the coaxial

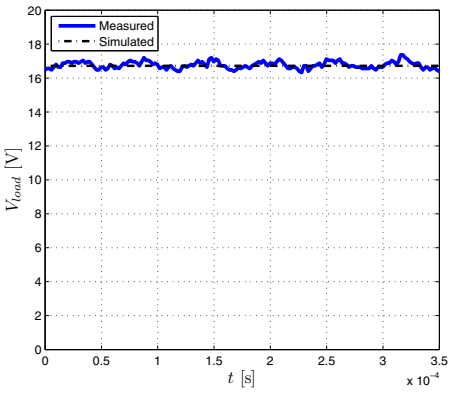

Fig. 16. Measured and simulated secondary voltage waveform across the load resistance for the adjacent winding topology.

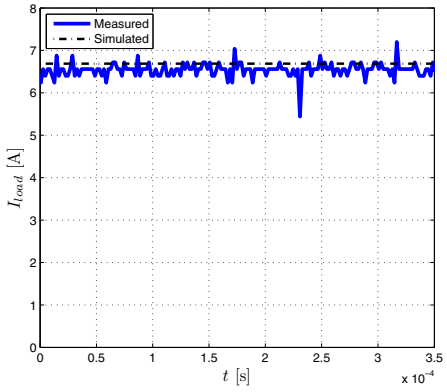

Fig. 17. Measured and simulated current waveform through the load resistance for the adjacent winding topology.

winding topology.

The power transfer of the manufactured transformer with the adjacent winding topology is measured in an experimental setup. The setup consist of a half-bridge which feeds the primary winding with high frequency voltage. A diode rectifier and an equivalent load of 2.5 Ohm are connected in series to the secondary winding. A stationary power transfer of 100 W has been obtained, due to limitation of the half bridge converter. The voltage and current waveforms across the equivalent load have been measured and simulated in MATLAB Simulink, and shown in Fig. 16 and Fig. 17, respectively. The measured and simulated voltage and current have the same amplitude.

Finally, a power transfer of 50 W is measured for different angular velocities, shown in Fig. 18. No significant difference in the power transfer is noticed for an increasing angular velocity.

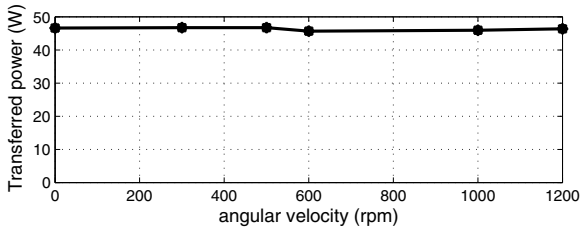

Fig. 18. Power transfer for different angular velocities.

VII. Conclusion

In this paper the adjacent and coaxial winding topologies in a rotating pot core transformer have been compared in terms of total core volume and power losses. A multi-objective optimization has been defined, using an electromagnetic and a thermal model of the rotating transformer. The optimization algorithm has been used to derive the minimal Pareto front, which showed that lower power losses could be obtained in the adjacent winding topology. Two prototype transformers have been designed and manufactured to verify the models. Performance measurements show no insignificant difference for an increasing angular velocity. Overall, the adjacent winding topology is favorable for a power transfer of 1 kW.

References

[1] A. Esser and H.-C. Skudelny, "A new approach to power supplies for robots," *IEEE Transactions on Industry Applications*, vol. 27, no. 5, pp. 872–875, 1991.

[2] K. Papastergiou and D. Macpherson, "An airborne radar power supply with contactless transfer of energy - part i: Rotating transformer," *IEEE Trans. Ind. Electron.*, vol. 54, no. 5, pp. 2874–2884, October 2007.

[3] D. Macpherson and K. Papastergiou, "Contact-less transfer of energy by means of a rotating transformer," *Proc. ISIE*, pp. 1735–1740, June 2005.

[4] J. Legranger, G. Friedich, S. Vivier, and J. Mipo, "Comparison of two optimal rotary transformer designs for highly constrained applications," *Electrical Machines & Drive Conference*, vol. 2, pp. 1546–1551, May 2007.

[5] K. Deb, *Multi-Objective Optimization using Evolutionary Algorithms*. WILEY, 2004.

[6] *FLUX 10 User's Guide*. Cedrat, 2009.

[7] F. van Horck, *A Treatise on Magnetics and Power Electronics*. Eindhoven University of Technology, 2006.

[8] W. Hurley, E. Gath, and J. Breslin, "Optimizing the ac resistance of multilayer transformer windings with arbitrary current waveforms," *IEEE Transactions on Power Electronics*, vol. 15, no. 2, pp. 369–376, 2000.

[9] J. de Boeij, E. Lomonova, and A. Vandenput, "Contactless energy transfer to a moving load part i: Topology synthesis and fem simulation," *IEEE International Symposium on Industrial Electronics*, vol. 2, pp. 739–744, July 2006.

[10] C. Wang, G. Covic, and O. Stielau, "Power transfer capability and bifurcation phenomena of loosely coupled inductive power transfer systems," *IEEE Transactions on Industrial Electronics*, vol. 51, no. 1, pp. 149–157, February 2004.

[11] Ferroxcube, *Data Handbook Soft Ferrites and Accessories*. Ferroxcube, November 2008.

[12] J. Holman, *Heat Transfer*. McGraw-Hill Book Company, 1986.

[13] D. V. Malyna, "Accelerated synthesis of electrically and thermally constrained power electronic converter systems," Ph.D. dissertation, Eindhoven Technical University, 2007.

[14] A. Messac, A. Ismail-Yahaya, and C. Mattson, "The normalized normal constraint method for generating the pareto frontier," *Structural and Multidisciplinary Optimization*, vol. 25, no. 2, pp. 86–98, 2003.